Resolving Inclusion Structure and Deformation Mechanisms in Polylactide Plasticized by Reactive Extrusion

Berit Brüster, Camilo Amozoqueño, Patrick Grysan, Inma Peral, Benjamin Watts, Jean-Marie Raquez, Philippe Dubois, and Frédéric Addiego*

A multiscale characterization approach is developed to resolve the structure of inclusions in polylactide (PLA) plasticized with acrylated poly(ethylene glycol) (acrylPEG) by reactive extrusion. Scanning transmission X-ray microscopy (STXM) coupled with near-edge X-ray absorption fine structure (NEXAFS) nanospectroscopy demonstrates that these inclusions have a core–shell morphology. This technique also proves that the inclusions consist of polymerized acrylPEG (poly(acrylPEG)), which is also confirmed by elastic modulus measurement using an atomic force microscope. The shell consists of poly(acrylPEG)-rich domains, while the core is less rich in the polymerized plasticizer. Upon drawing, the density of the inclusion's core and shell markedly decreases as shown by microcomputed X-ray tomography measurements, and no inclusion–matrix debonding is observed. At the same time, sub-micrometer cracks are noted between inclusions by STXM/NEXAFS imaging, which may result from the presence of crosslinking points restricting the local chain mobility. Novel knowledge about the reactive extrusion-induced PLA structure is released.

1. Introduction

Polymer reactive processing is considered as a flexible, fast, and solvent-free method to create polymer-based materials with new functions and/or properties, and hence, with a new performance during their application. Through chemical reactions of a polymer matrix with other reactants, extrusion enables, for example, free radical grafting of monomers/oligomers onto the polymer backbone, polymerization when starting from monomers or prepolymers, and reactive polymer blending from immiscible polymers.[1–3] The grafting of oligomers is for example commonly done to increase the plasticity of brittle polymers at room temperature. In this context, polylactide (PLA) was extruded with oligomeric reactive plasticizers in the presence of a free radical initiator yielding to a plasticized PLA.[4–7] As plasticizers, tributyl citrate (TBC),[4] poly(ethylene glycol) methyl ether methacrylate (MAPEG),[5] and poly(ethylene glycol) methyl acrylate (acrylPEG)[5–7] were successfully used resulting in an improved elongation at break of these plasticized PLA compared to the reference PLA.

One of the challenges of reactive processing is to identify the chemical structure of the obtained polymers due to the very local scale at which transformations occurred. Most of the time, a multiscale approach was used to characterize the structure of the as-processed polymers.[5,7] In the case of PLA plasticized with acrylPEG as a reactive plasticizer and a free radical initiator (Luperox L101), the resulting material was named plasticized PLA (pPLA). pPLA structure was analyzed to be a PLA matrix plasticized by partially grafted and partially free inclusions of polymerized acrylPEG oligomers. The free radical initiator induced two possible reactions: (i) the polymerization of the acrylPEG plasticizer to form free inclusions and (ii) the formation of a PLA radical as a starting point for the polymerization of acrylPEG to create grafted inclusions. In addition, a low content of crosslinking was observed by polymerized plasticizer molecules that grafted onto two PLA units or by recombination of two radicals.[5,7] The grafting of the plasticizer onto PLA backbone was indirectly proved by an increase of melt viscosity during the reactive extrusion, the presence of a nonextracted fraction of plasticizer after Soxhlet extraction of the pPLA with methanol, and an extensive molecular characterization.[5] Note that the extracted fraction after Soxhlet extraction of the pPLA proved the existence of free plasticizer oligomers within the PLA matrix.[5,7] Concerning crosslinking, swelling testing of the pPLA in chloroform resulted in a gel formation, demonstrating the occurrence of a crosslinked molecular network.[7] Only a little attention was paid to the characterization of the inclusion's chemical structure and the related mechanical behavior. One of the main reasons relies on the fact that plasticizer

B. Brüster, C. Amozoqueño, P. Grysan,
Prof. P. Dubois, Dr. F. Addiego
Department Materials Research and Technology (MRT) and
National Composite Centre – Luxembourg (NCC-L)
Luxembourg Institute of Science and Technology (LIST)
ZAE Robert Steichen, 5 Rue Bommel, 4940 Hautcharage, Luxembourg
E-mail: frederic.addiego@list.lu

Dr. I. Peral
Faculté des Sciences
de la Technologie et de la Communication
Université du Luxembourg
Campus Limpertsberg, 162a Avenue de la Faïencerie
1511 Luxembourg, Luxembourg

Dr. B. Watts
Paul Scherrer Institute, 5232 Villigen-PSI, Switzerland

Dr. J.-M. Raquez
Laboratory of Polymeric and Composite Materials (LPCM)
Centre d'Innovation et de Recherche en Matériaux Polymères (CIRMAP)
Université de Mons
Place du Parc, 20, 7000 Mons, Belgium

polymerization and grafting and/or crosslinking reactions may occur at the same time making the interpretation of the inclusion structure difficult. Another reason relies on the very local scale at which all these transformations occurred requiring cutting-edge characterization tools that provide information at the nanometer and sub-micrometer scales. Nevertheless, identifying inclusion chemical structure may provide some novel knowledge about reactive extrusion mechanisms, which may help to further optimize this advanced process. Studying the local inclusion mechanical behavior may also contribute to the understanding of the overall mechanical behavior of pPLA, as it is the case for rubber-toughened polymers in general. For example, in high-impact polystyrene (HIPS), the presence of inclusions with a rubber-like behavior acted as craze initiator and provided further plasticity before rupture compared to the reference polystyrene.[8]

The objective of the current paper was to analyze the chemical structure and the resulting mechanical behavior of plasticizer inclusions in PLA modified by reactive extrusion with acrylPEG. Scanning transmission X-ray microscopy (STXM) equipped with near-edge X-ray absorption fine structure (NEXAFS) nanospectroscopy was recently applied with success to identify the most representative chemical bond of inclusions dispersed within a PLA matrix.[9] STXM/NEXAFS was hence utilized in our works to identify the most representative chemical bond of the plasticizer inclusion and to analyze its local distribution. Then, information about the elastic modulus of the inclusions was obtained by means of an atomic force microscope (AFM) equipped with a nanomechanical module.[10] Last, inclusion's deformation mechanisms were qualitatively analyzed after drawing by STXM/NEXAFS and microcomputed X-ray tomography (µCT).

2. Experimental Section

The PLA grade reference 4043D was purchased from Nature-Works (Minnetonka, MN, USA). It was characterized by a D-isomeric unit content of 4.2 mol%. As in previous works,[5,7] acrylPEG ($M_n \approx 480$ g mol^{-1}) from Sigma-Aldrich (Steinheim, Germany) was selected as the reactive plasticizer, while Luperox 101 (L101) from Sigma-Aldrich (Steinheim, Germany) was used as a free radical initiator. Prior to extrusion, PLA pellets were dried at 50 °C overnight. The reactive extrusion of PLA was conducted by means of a twin-screw miniextruder Haake Rheomex OS PTW 16 manufactured by Thermo Scientific (Karlsruhe, Germany). This extruder was coupled with the motor Haake PolyLab OS drive from Thermo Scientific (Karlsruhe, Germany) and had a screw diameter D of 16 mm. The barrel length L was configured to get an L/D ratio of 40 suitable for long reactive extrusion experiments. Note that the processing conditions selected here yielded a residence time of 5 min. The reactive extrusion procedure consisted of these successive stages: (i) 50 g of PLA/acrylPEG/L101 mixture with compositions 79/20/1 in wt% was prepared and manually mixed in a beaker, (ii) the mixture was manually introduced in the first feed aperture of the extruder that was set at 200 °C in every zone, while screw speed was set to 100 rpm, (iii) the obtained strands were cooled to room temperature in air and pelletized, (iv) the pellets were

introduced in a gravimetric micro twin-screw feeder Brabender (Duisburg, Germany) set to a feeding rate of 20% (corresponding to 1.3 kg h^{-1}), and (v) the pellets were finally extruded at 200 °C (all zones) at 100 rpm into films with a thickness of about 0.2 mm by means of a sheet die coupled with a contact roller positioned onto a conveyor belt. In the case of PLA and the simple blending between PLA and acrylPEG, only one extrusion step was conducted. The following formulations of PLA/acrylPEG/L101 were prepared (composition in wt%): 100/0/0 (PLA), 80/20/0 (PLA/acrylPEG, plasticized by blending), and 79/20/1 (pPLA, plasticized by reactive extrusion). Note that a reactive extrusion of acrylPEG with L101 (poly(acrylPEG)) with weight composition 95/5 was processed by means of a micro-compounder DSM Xplore 15 cc (Geleen, Netherlands) with a nitrogen purge. In this case, extrusion was conducted at 180 °C at a screw speed of 50 rpm during 5 min, producing gel-like strands of diameter comprised between 3 mm and 5 mm.

The possible reactions during the reactive extrusion as described in recent works are represented in **Figure 1**.[5,6] First, the thermal degradation of the peroxide bond in the initiator L101 resulted in the formation of free radicals represented by R-O·. Second, these radicals of the initiator created radicals on the PLA backbone. Third, the PLA backbone radicals would initiate the acrylPEG grafting followed by polymerization, yielding grafted poly(acrylPEG). The fourth reaction indicated the formation of poly(acrylPEG) without grafting onto the PLA backbone, which was directly started by the radical initiator.

The thermal properties of the PLA-based materials were measured by differential scanning calorimetry (DSC) with a Netzsch DSC 204 F1 (Selb, Germany). To this end, samples with a mass comprised between 3 and 5 mg were cut from the films and subjected first to a cooling stage from room temperature to –100 °C at a rate of –10 °C min^{-1}, and then the samples were heated at 180 °C with a rate of 10 °C min^{-1}. The glass transition temperature (T_g), the cold-crystallization temperature (T_{cc}), the cold-crystallization enthalpy (ΔH_{cc}), the melting temperature (T_m), and the melting enthalpy (ΔH_m) of the samples were obtained from this first heating stage to get the properties of the as-processed materials. The crystallinity was calculated based on Equation (1) where x_{PLA} was the total weight amount of PLA (79 wt% for pPLA, 80 wt% for PLA/acrylPEG, and 100 wt% for PLA), and $\Delta H_{m,0}$ was the melting enthalpy of a 100% crystalline PLA determined to be $\Delta H_{m,0} = 93$ J g^{-1}[11]

$$X_c = \frac{\Delta H_m - \Delta H_{cc}}{x_{PLA} \times \Delta H_{m,0}} \tag{1}$$

A miniature tensile/compression module Kammrath & Weiss (Dortmund, Germany) was utilized to highlight the different tensile behaviors of the materials. This machine was equipped with a 5 kN load cell (1 N of resolution within all the load range) and a linear variable differential transformer enabling to measure sample displacement ΔL. The dumbbell-shaped specimen were cut from the extruded film with their axis oriented parallel to the extrusion direction. Their initial gauge length L_o was about 37 mm, and their width in the gauge section W_o was about 5 mm (exact values were measured for each sample). Drawing of the samples was conducted at 22 °C with a crosshead displacement speed $\Delta L/\Delta t$ of 10 µm s^{-1}. The

Figure 1. Chemical structures of the possible reactions during the reactive plasticization of PLA with acrylPEG as plasticizer and L101 as free radical initiator: (I) structure of L101 and thermal degradation of the initiator to radical, (II) radical formation on the PLA backbone, (III) grafting of acrylPEG onto the PLA backbone followed by polymerization, and (IV) polymerization of acrylPEG to poly(acrylPEG).

engineering strain ε_{eng} (in %) was calculated as $100 \cdot \Delta L/L_0$, and the corresponding strain rate $\Delta \varepsilon /\Delta t = 1/L_0 \cdot \Delta L/\Delta t$ was evaluated to be 2.7×10^{-4} s^{-1}. The engineering stress σ_{eng} was calculated from the measured load divided by the initial cross-section S_0. The Young's modulus E of the materials was calculated from the initial slope $d\sigma_{eng}/d\varepsilon_{eng}$ of the tensile curves. PLA, pPLA, and PLA/acrylPEG samples were drawn to a maximum engineering strain of about 16%, corresponding to the limit of the machine with a gauge length of 37 mm. In the case of pPLA, inclusion deformation mechanisms were studied from samples drawn to a maximum engineering strain of 15% and unloaded to zero stress resulting in an engineering strain of 12%. It was noted that pPLA-drawn samples exhibited important whitening at their center.

AFM measurements were done by means of an Asylum MFP3D Infinity (Santa Clara, California) in fast force mapping, which allowed the recording of topography and a force curve at each pixel of the 256 pixels × 256 pixels images at a line speed from 0.5 to 1 Hz. For this characterization, the samples cut from the extruded films were melted against a glass slide at 180 °C and then were slowly cooled to room temperature in air. This procedure enabled to obtain a reasonable flat surface

for the AFM measurements. Prior to measurements, tips' cantilever force constant was calibrated with a Sadler noncontact method. The calibration was further checked by the analysis of a known polycarbonate reference sample (from Asylum) with an elastic modulus of 2.5 GPa. Different cantilever stiffnesses were chosen in function of the elastic moduli of the inclusion. Accordingly, PLA, pPLA, and PLA/acrylPEG were analyzed with ACT160TS (37 N m^{-1}), ACT240TS (2 N m^{-1}), and TR800PSA (0.7 N m^{-1}), respectively. On each image, at least five zones were picked up within the matrix and the inclusions, the choice being made in function of the local topography with a preference for flat surfaces. For the inclusion, the force curves were extracted by Asylum retreatment software and fitted with Hertz punch model for pPLA and with Oliver–Pharr model for PLA/acrylPEG to extract the elastic modulus.

The STXM experiments coupled with NEXAFS nanospectroscopy were performed at the PolLux beamline at the Swiss Light Source (Paul Scherrer Institute, Villigen, Switzerland).[12] Some details about the technique used were found in the literature.[13] Briefly, a Fresnel zone plate focused the monochromatic synchrotron X-ray beam onto a small spot (less than 30 nm) on the sample, while the transmitted X-rays were measured by

a photomultiplier tube coupled with a scintillator screen. The relative position of the zone plate (hence the focused spot of the X-ray beam) and the sample was measured by an interferometer and coupled to the piezo-driven scanning stage to ensure positioning stability and reproducibility. The experiments were conducted under high vacuum (about 10^{-6} mbar). All STXM samples, excepted poly(acrylPEG), were cut into 100 nm thick lamellae by means of a cryo-ultramicrotome Leica EM UC6/UF6 (Wien, Austria) that was operated at −30 °C. Samples were cut into thin lamellae by wet sectioning with a diamond knife using a dimethyl sulfoxide/water mixture (60/40 vol%) before being transferred onto copper grids. In the case of poly(acrylPEG), it was not possible to prepare thin lamellae by wet-sectioning due to the high solubility/swellability of this material with water. Hence, poly(acrylPEG) was directly dissolved in water, dropped on the copper grid, and dried at room temperature. The copper grids carrying samples were mounted on an earthed metal sample plate and positioned to be in the focal position of the monochromatic X-ray beam. Composition maps were calculated from transmission images taken at photon energies of 280 eV (pre-edge), 288.5 eV (PLA resonance), 289.7 eV (acrylPEG resonance), and 320 eV (chemically insensitive). The aXis2000 software package (McMaster University, Hamilton, ON, Canada) was used for the data analysis.

μCT testing was directly conducted on a drawn pPLA tensile sample to investigate the structure of the material. The equipment used was a Xradia 510 Versa 3D X-ray Microscope from Zeiss (Pleasanton, CA, USA) enabling a spatial resolution of about 1 μm whatever the sample position relative to the X-ray source. The μCT images were recorded during 19.5 h at 40 kV, 3 W, and with a 40× objective. One area at the center of the tensile specimen at the most deformed zone (where intense whitening was observed), and one area at a not or little-deformed zone of the tensile specimen (transparent area) were scanned. The two volumes were reconstructed with a 0.3 μm voxel size. Note that only 2D images were extracted from the reconstructed volume corresponding to a slice taken at the center of each volume.

3. Results and Discussion

3.1. Initial Properties of PLA-Based Materials

Before investigating the inclusion's structure, it was necessary to determine the overall thermal properties of the PLA-based materials, which are reported in **Table 1**. While PLA exhibited a T_g of 62.5 °C and a T_m of 150.4 °C, its melting enthalpy was just slightly higher than the cold-crystallization enthalpy that

occurred at a temperature of 118.6 °C, providing a very low crystallinity of around 4.6 wt%. Reactive plasticization with acrylPEG caused a significant decrease of T_g attaining 36.4 °C compared to PLA. On the DSC thermogram of PLA/acrylPEG, just a poorly visible glass transition at 11.4 °C was observed. Since the oligomeric acrylPEG offers no glass transition temperature and a melting point slightly below 0 °C, this glass transition temperature was attributed to the glass transition of the blended material. PLA/acrylPEG's T_g was below room temperature and, hence, much lower as for PLA and pPLA. The cold-crystallization temperature of pPLA and PLA/acrylPEG was comparable and close to 76 °C, which was much lower than for PLA. In both plasticized materials, the cold-crystallization enthalpy was lower than that of PLA, and the melting enthalpy was higher. This resulted in a higher crystallinity for the plasticized samples. As reported in the literature,[5–7] plasticization drastically increased the chain mobility of PLA, explaining the decrease of T_g and T_{cc}, as well as the increase of X_c. It is important to highlight the different structures of the two plasticized samples. While PLA/acrylPEG is a blend of PLA and the plasticizer acrylPEG without any chemical reaction between the matrix and the plasticizer, in pPLA the chemical grafting of the plasticizer created a unique structure as already described in the literature: The polymerization of acrylPEG to poly(acrylPEG) led to grafted or free inclusions in the PLA matrix and grafting of poly(acrylPEG) onto two PLA sites induced a slight crosslinking in the material.[5,14] The DSC thermogram of poly(acrylPEG) shows a glass transition at −60.4 °C as already reported,[5] and a melting peak at −1.9 °C, which is slightly below 0 °C as the melting point of nonpolymerized acrylPEG. The absence of a separated melting peak in PLA/acrylPEG and pPLA supports the assumption of a good miscibility between the plasticizer and the matrix even after reactive plasticization.

The tensile behavior of PLA, pPLA, and PLA/acrylPEG is represented in **Figure 2**. It can be noted that the plasticization method drastically influences the engineering stress—engineering strain curve of PLA. First, Young's modulus increases in this material order: PLA/acrylPEG (321 MPa) < pPLA (1250 MPa) < PLA (3690 MPa). After the initial viscoelastic stage, all the materials exhibit viscoplasticity with a yield stress that increases in this material order: PLA/acrylPEG (7.5 MPa) < pPLA (21 MPa) < PLA (38 MPa). Last, PLA has a quite low elongation at break corresponding to an engineering strain of 3%, while the two plasticized PLA have an elongation at break higher than the limit of the machine (>16%). The two plasticization methods clearly decrease the rigidity and increase the ductility of PLA. Nevertheless, reactive plasticization provides a material with a higher rigidity and strength compared to the plasticization by blending. This result can be explained by

Table 1. Thermal properties of PLA-based materials determined by DSC obtained from the first heating stage (with standard deviations).

Material	T_g [°C]	T_{cc} [°C]	T_m [°C]	ΔH_{cc} [J g^{-1}]	ΔH_m [J g^{-1}]	X_c [wt%]
PLA	62.5 ± 0.2	118.6 ± 0.1	150.4 ± 0.3	18.9 ± 0.3	23.2 ± 0.9	4.6 ± 1.2
PLA/acrylPEG	11.4 ± 1.6	75.6 ± 1.6	150.6 ± 0.4	14.3 ± 1.1	25.0 ± 0.2	14.5 ± 1.3
pPLA	36.4 ± 0.6	76.4 ± 1.1	146.1 ± 1.3	15.4 ± 0.1	25.3 ± 0.3	13.5 ± 0.5
poly(acrylPEG)	−60.4 ± 0.5	−34.7 ± 0.2	−1.9 ± 0.6	26.3 ± 07	28.7 ± 0.9	–

**ADVANCED
SCIENCE NEWS**

www.advancedsciencenews.com

**Macromolecular
Materials and Engineering**

www.mme-journal.de
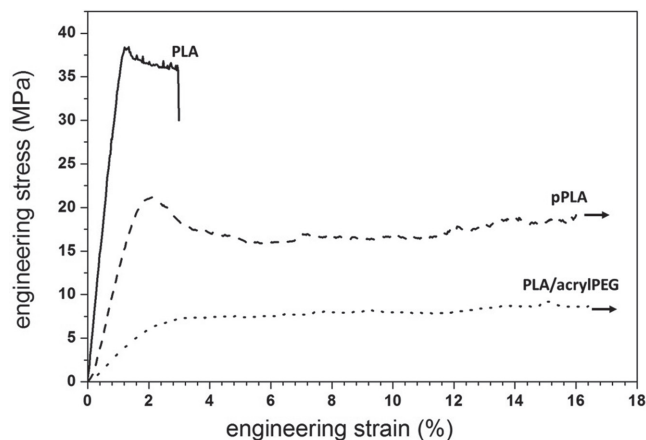
Figure 2. Representative tensile curves of PLA (solid), pPLA (dash), and PLA/acrylPEG (dot) tested at 22 °C and 2.7×10^{-4} s^{-1}.

the difference in glass transition temperature between pPLA (36.4 °C) and PLA/acrylPEG (11.4 °C), and by the presence of crosslinks in pPLA.

3.2. Inclusion Chemical Structure

The chemical structure of the inclusions in pPLA was examined by STXM/NEXAFS and compared to that of the pPLA matrix, the PLA/acrylPEG matrix, neat PLA, and poly(acrylPEG) (**Figure 3**). First, C1s NEXAFS spectra of pPLA inclusion and pPLA matrix were compared in order to identify a photon energy displaying differences in the X-ray absorption that could be utilized to differentiate these materials (Figure 3a). In the case of pPLA matrix, a strong resonance peak was noted at 288.5 eV. It was assigned to the C1s → $\pi^*_{(C=O)}$[9,15] and was obviously one of the most representative chemical functions in PLA monomer unit (peak labeled 1). Another resonance peak appeared at 289.9 eV and was commonly attributed to the C1s → C-H Rydberg states (peak labeled 2).[9,16] Last, some resonance peaks observed in the range of 292 to 300 eV were probably associated with C1s → $\sigma^*_{(C-C)}$ transitions.[9,17] In the case of pPLA inclusions, two main resonance peaks centered at

288.8 and 289.7 eV were noted. Based on NEXAFS testing done on oligo(ethylene glycol) and PEG-based plasma polymer, the resonance at 288.8 eV can be attributed to C1s → $\pi^*_{(C-H)}$ transition (peak labeled 3), while the resonance at 289.7 eV can be attributed to the C1s → $\sigma^*_{(C-O)}$ transition (peak labeled 4).[18,19] Additional resonance peaks were observed for the inclusion in pPLA in the range of 292 to 300 eV and assigned probably to C1s → $\sigma^*_{(C-C)}$ transition.[9,17] Note that the weak resonance at 285.2 eV was attributed to some carbon contamination.[20]

When comparing the pPLA inclusion spectrum with the pPLA matrix spectrum, it can be clearly seen that the energy of peak labeled 1 (C1s → $\pi^*_{(C=O)}$ of the matrix) can be used to highlight PLA-rich domains, while the energy of peak labeled 4 (C1s → s$^*_{(C-O)}$ of the inclusion) can be used to highlight plasticizer-rich domains. By comparing the pPLA matrix spectrum with that of PLA/acrylPEG matrix and neat PLA, no significant difference was noted (Figure 3b), indicating that the chemical modifications of PLA matrix (grafting and crosslinking with the plasticizer) were not detected by STXM/NEXAFS. More interestingly, the spectrum of poly(acrylPEG) was similar to the one of pPLA's inclusions (Figure 3b), with the previously suggested reaction mechanism that acrylPEG polymerizes to form inclusions.[5,6]

STXM images recorded at 288.5 eV (PLA-rich domains) and at 289.7 eV (poly(acrylPEG)-rich domains) in the case of pPLA were shown in **Figure 4**. PLA-rich domains were obviously observed in the matrix (Figure 4a,c,e), while inside the inclusions, only some small areas of these PLA-rich domains were noted (Figure 4c). Concerning the poly(acrylPEG)-rich domains, they were obviously localized within the inclusions (Figure 4b,d,f). One important result was that inside the inclusion, the distribution of these poly(acrylPEG)-rich domains was heterogeneous. In particular, these domains appeared to be localized at the inclusion shell (Figure 4b,f), or are randomly distributed in the rest of the inclusion, especially for the large inclusions (Figure 4d). To understand the inclusion structure obtained by STXM/NEXAFS, it is important to consider the sample preparation methodology of slicing 100 nm-thick specimens. It was hypothesized that a core–shell structure exists in pPLA inclusions. When the specimen cutting passed through the equatorial region of an inclusion, then a perfect core–shell effect may be visible as in Figure 4f. The inclusion shell would
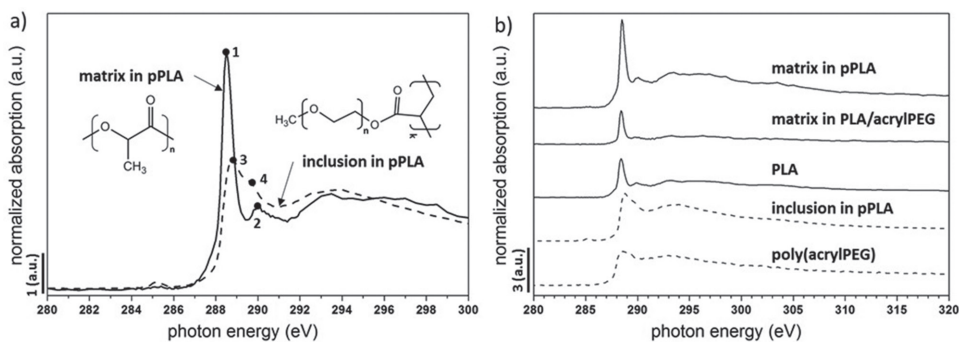
Figure 3. a) C1s NEXAFS spectrum of pPLA inclusion compared to that of pPLA matrix (with the corresponding chemical structures); b) C1s NEXAFS spectra of pPLA matrix, PLA/acrylPEG matrix, neat PLA, pPLA inclusion, and neat poly(acrylPEG). All the spectra were extracted and reduced from STXM images. 1: C1s → $\pi^*_{(C=O)}$ of the pPLA matrix, 2: C1s → C-H Rydberg of the of the pPLA matrix, 3: C1s → $\pi^*_{(C-H)}$ of the pPLA inclusion, and 4: C1s → $\sigma^*_{(C-O)}$ of the pPLA inclusion.

ADVANCED
SCIENCE NEWS
www.advancedsciencenews.com

Macromolecular
Materials and Engineering
www.mme-journal.de
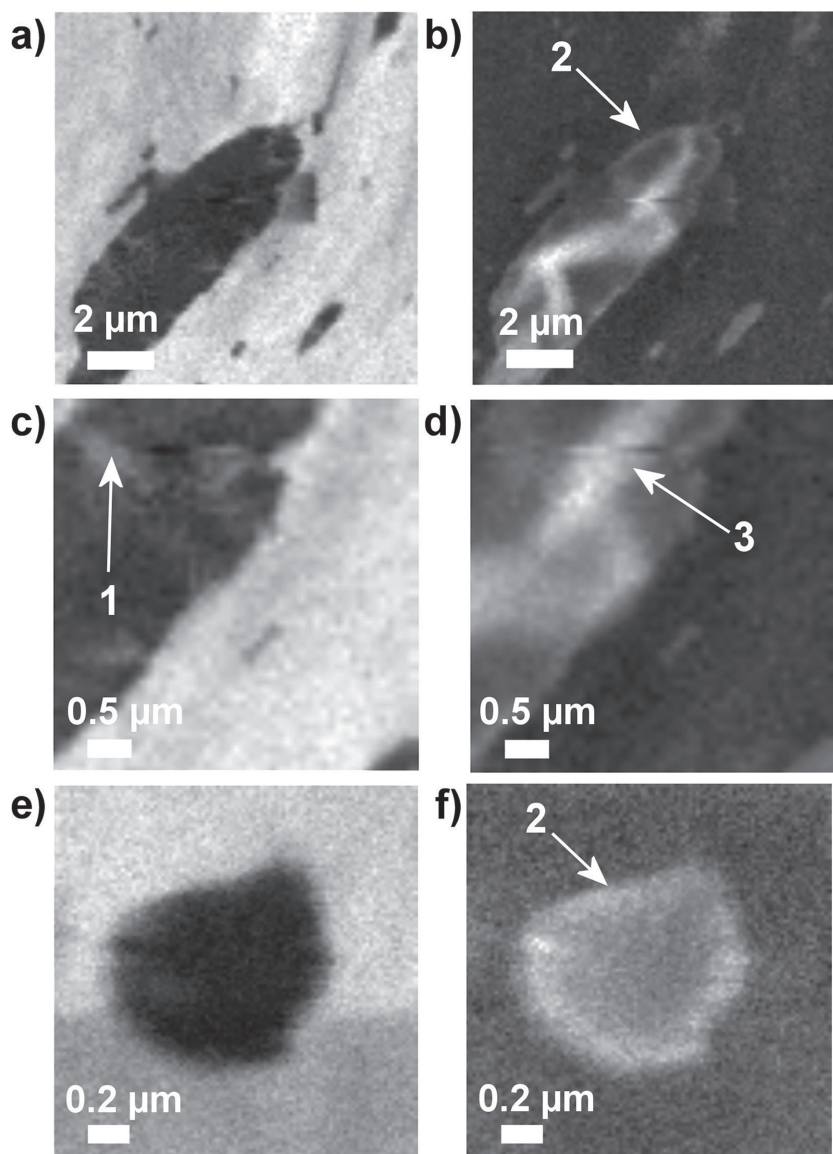
Figure 4. Composition maps obtained from STXM images of pPLA indicating the present amount of a,c,e) PLA, and b,d,f) poly(acrylPEG). Images (a) to (d) represented the same area at different magnifications, while images (e) and (f) were taken in another area of interest. 1: PLA-rich domains inside the inclusion, 2: poly(acrylPEG)-rich domains at the inclusion shell, and 3: poly(acrylPEG)-rich domains at the inclusion core.

of the plasticizer and free radical initiator injection into the extruder, the liquids were heated and distributed/dispersed within the melted PLA matrix under shear and elongational flows. When the radical initiator attained its decomposition temperature, free radicals were formed and radical reactions occurred in all of the material. As described in by Kfoury and colleagues,[5] the free radical initiator can create radicals in the PLA backbone chain or can polymerize the acrylPEG to poly(acrylPEG). Furthermore, the formed PLA radicals can also start the polymerization of acrylPEG so that poly(acrylPEG) exists grafted onto the PLA backbone, and the recombination of radicals or grafting of poly(acrylPEG) twice to the PLA matrix induced crosslinking. The localization of poly(acrylPEG) at the shell of the inclusions is hard to explain by a mechanism, because the radical reactions are uncontrollable and, in addition, the material underlay shear forces in the extruder. It was assumed that the plasticizer forms agglomerates in the viscous PLA matrix so that reactions at the interface between the agglomerates and the PLA matrix were preferred. Indeed, in this area free radicals engendered from the radical initiator, acrylPEG, and PLA are present, which enhance reactivity. It is however to be noted that the grafting and crosslinking bonds between the plasticizer and the matrix can at a given point of the reactive extrusion decrease the mobility and could hinder the formation of more dense inclusions (Figure 4f).

3.3. Inclusion Mechanical Behavior

The mechanical behavior of PLA-based materials was first investigated by AFM imaging. In this context, the coupling between topographical contrast imaging and elastic modulus contrast imaging of PLA, PLA/acrylPEG, and pPLA was represented in **Figure 5**. The average elastic modulus of the matrix and inclusions was reported in **Table 2**. Concerning PLA, an average matrix elastic modulus of 2.40 ± 0.26 GPa was obtained (Figure 5b). In the case of pPLA, the presence of holes and nanometric inclusions was observed (Figure 5c). The average elastic modulus of the pPLA matrix was 2.60 ± 0.26 GPa, while that of the inclusions was 0.23 ± 0.04 GPa. The presence of holes may be due to the destruction of plasticizer inclusion shells during sample preparation, highlighting again the possible core–shell effect. The AFM investigation of PLA/acrylPEG was much more complicated due to the leaching of plasticizer at the sample surface. As shown by DSC, PLA/acrylPEG has a T_g below room temperature and behaves hence rubber-like at room temperature.

be in this case from poly(acrylPEG)-rich domains, while the inclusion core would be less rich in poly(acrylPEG). In the case where the specimen cutting would pass near a border region of the inclusion, the resulting structure would mainly consist of the poly(acrylPEG)-rich domains. However, the cutting procedure could lead to a damage of the inclusions structure, resulting in a heterogeneous structure as shown in Figure 4b. Note that the presence of PLA-rich domains in the inclusion (Figure 4c) was expected to be due to the cutting procedure that may extract some PLA from the matrix.

To understand the core–shell structure of pPLA inclusions, the processes involved in producing the material have to be examined. It can be hypothesized that during the first seconds

ADVANCED
SCIENCE NEWS
www.advancedsciencenews.com

Macromolecular
Materials and Engineering
www.mme-journal.de

Figure 5. AFM investigation of a,b) PLA, c,d) pPLA, and e,f) PLA/acrylPEG with topographical contrast mode (a, c, and e) and modulus contrast mode (b, d, and f). The circles and squares represented the areas where elastic modulus was calculated.

The migration of the plasticizer to the surface was observed since the simple blending of PLA and acrylPEG formed no inclusions of grafted plasticizer. The observed areas of plasticizer were agglomerations of leached plasticizer, which complicated the separated analysis of matrix and plasticizer phase only done on a limited number of areas (Figure 5e,f). The average elastic modulus of PLA/acrylPEG matrix was 1.79 ± 0.10 GPa, while that of its plasticizer phase was 0.04 ± 0.01 GPa. This

Table 2. Average elastic modulus of the matrix and inclusion calculated by AFM for PLA, PLA/acrylPEG, and pPLA (with standard deviations).

Material	Averaged elastic modulus [GPa]	
	Matrix	Inclusion
PLA	2.40 ± 0.26	–
PLA/acrylPEG	1.79 ± 0.10	0.04 ± 0.01
pPLA	2.60 ± 0.26	0.23 ± 0.04

nanomechanical study of PLA-based materials revealed that the plasticizer's elastic modulus increased by a factor of 475% from PLA/acrylPEG to pPLA that is clearly a further evidence for the acrylPEG polymerization, in addition to the STXM/NEXAFS results (Figure 3b). Note that here only poly(acrylPEG) inclusions with a faultless shell could be analyzed, which were difficult to find. Indeed, most of the supposed inclusions were holes in the case of pPLA (Figure 5c), which did not permit the determination of the inclusion elastic modulus. The weak increase of elastic modulus of the matrix from PLA to pPLA may be due to the local grafting/crosslinking points of PLA with poly(acrylPEG) and to the increased crystallinity (Table 1). On the contrary, the decrease of matrix elastic modulus from PLA to PLA/acrylPEG may be due to the local dispersion of acrylPEG plasticizer within the PLA matrix that overcame the gain in rigidity due to the increase of matrix crystallinity.

The 2D composition maps obtained from STXM images of deformed pPLA recorded at 288.5 eV (PLA-rich domains) and

**ADVANCED
SCIENCE NEWS**
www.advancedsciencenews.com

**Macromolecular
Materials and Engineering**
www.mme-journal.de
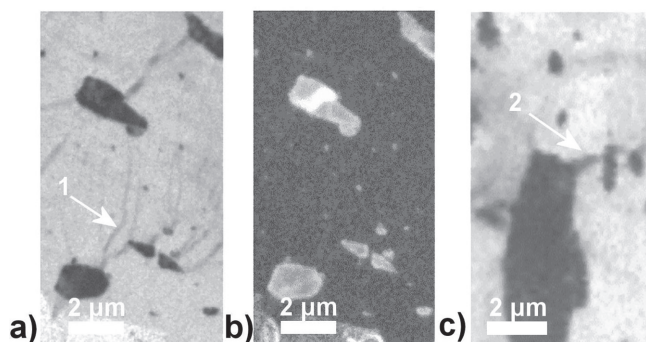
Figure 6. Composition maps obtained from STXM images of pPLA at a strain level of 12% indicating the present amount of a) PLA and b) poly(acrylPEG) in a first area, and c) PLA in a second area. Tensile axis is diagonal (about 45° diagonally from the upper left to lower right). 1: sub-micrometer crack at the vicinity of inclusions of plasticizer and 2: sub-micrometer crack originated from one inclusion and propagating to a neighboring inclusion.

289.7 eV (poly(acrylPEG)-rich domains) were represented in **Figure 6**. Damage characterized by sub-micrometer defects oriented perpendicular to tensile direction was observed at the vicinity of plasticizer inclusions (Figure 6a). Such defects have never been detected in pPLA with other techniques.[21] From the 2D composition map in Figure 6a, it was not clear whether damage was generated in the matrix or from the inclusions. In another area (Figure 6c), it can be seen that damage was originated from one inclusion and propagated to a neighboring inclusion. Knowing this mechanism and coming back to Figure 6a, it was clearer that the defects started from one inclusion and propagated to another inclusion, but on the overall, damage remained localized. In the case of poly(acrylPEG)-rich domain image (Figure 6b), the core–shell structure of the inclusions was preserved after drawing without any particular damage, which was suitable. The observed defects were considered as sub-micrometer cracks and not sub-micrometer crazes. Indeed, in PLA, the tensile deformation induces crazes in the matrix, which can be observed by small-angle X-ray scattering (SAXS) testing as two perpendicular scattering streaks on the patterns.[22,23] However, in the case of the pPLA, no scattering streak was observed in SAXS patterns (results not shown here). The presence of inclusions acted as stress concentration points upon drawing inducing damage. In PLA blended with rubber particles, the localization of stress-induced crazing initiated by the rubber inclusions.[24] Crazing was in this case followed by internal cavitation of the rubber particles, these two damage mechanisms enabling further plasticity compared to neat PLA. Similar observations were made in HIPS.[8] In the case of pPLA, the reactive blending of PLA with acrylPEG engendered crosslinking points between the plasticizer and the matrix. Such crosslinking points may locally hinder fibrillation to dissipate stress around the inclusions explaining the occurrence of cracking instead of crazing, which

was a priori not suitable concerning plasticity.[25] Generally, cracks can quickly propagate and coalesce engendering material failure, while crazing may better dissipate stress than cracking due to internal fibril rearrangement enhancing plasticity. Nevertheless, the observed sub-micrometer cracks appeared localized between inclusions and did not propagate further, which was a posteriori desirable for ensuring a good plasticity.

Complementary information about the mechanical behavior of the plasticizer inclusion was obtained by µCT testing performed on a drawn tensile specimen of pPLA (**Figure 7**a). In particular, the center of the tensile specimen (the most deformed area), and a nondeformed or little-deformed area were analyzed (Figure 7b,c). The 2D image recorded for a little or nondeformed area of pPLA exhibited a quite homogeneous contrast of X-ray absorption (Figure 7b). It was not possible to distinguish the inclusions from the PLA matrix due to the lack of density contrast and/or limitation in spatial resolution (about 1 µm) of µCT that did not permit to visualize the inclusions. In the case of the most deformed area of pPLA, the 2D image recorded at the core of tensile specimen exhibited a totally different aspect compared to the previous case. Indeed, an important density of ellipsoids oriented in the tensile direction with a dark contrast was observed (Figure 7c, zone labeled 1). These ellipsoids had a lower density than the matrix and, hence, appeared as voids by µCT due to the limited spatial resolution of this equipment and/or to the low density of the inclusion core that did not absorb X-ray. The core–shell structure, which was already observed in the STXM/NEXAFS results (Figure 4), was also present in the µCT image of the deformed zone (Figure 7c, zone labeled 2). It can be concluded that drawing caused an important decrease of the density in the poly(acrylPEG)-poor core, as well as in the poly(acrylPEG)-rich shell of the inclusions since both are clearly visible compared to the nondeformed area (Figure 7b,c). This finding confirmed our previous results obtained by means of a scanning transmission electron microscope.[21] The deformation impacted both the inclusion's core and its shell resulting in a decrease of density, and no inclusion–matrix debonding was noted. The observed deformation mechanism of plasticizer inclusion is hence suitable for increasing PLA plasticity by locally dissipating stress without internal damage and inclusion–matrix
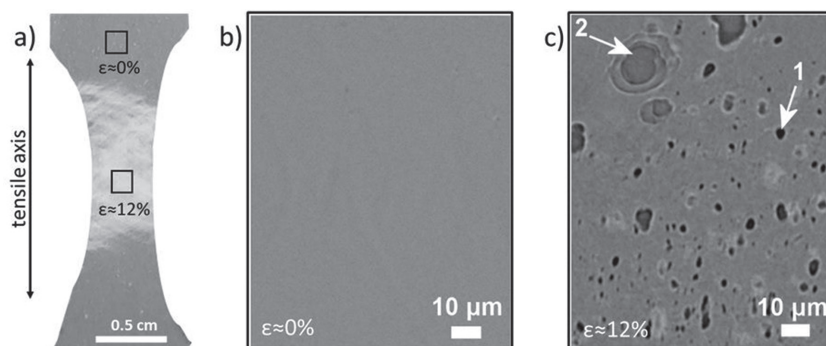
Figure 7. a) Picture of a drawn tensile sample of pPLA at a strain of 12% with the two areas marked for the 2D µCT images recorded in b) a nondeformed or little deformed area and c) the most deformed area (both µCT images were recorded with a spatial resolution of about 1 and 0.3 µm of voxel size). Tensile axis is vertical. 1: inclusion without density contrast, 2: inclusion with a density contrast indicating the presence of the shell.
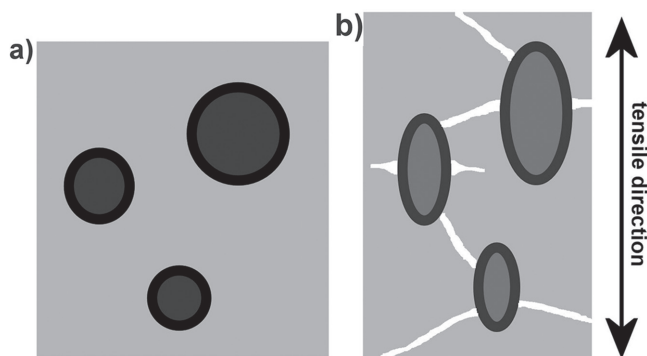
Figure 8. Schematic representation of pPLA inclusion structure a) prior drawing showing the core–shell morphology and b) after drawing characterized by a marked decrease of the density of the inclusion core as well as inclusion shell and by the formation of cracks bridging the inclusions.

debonding. It is worth to mention that the resolution of this technique restricted to observe the cracks between the inclusions as observed before by STXM (Figure 6). Furthermore, shear bands were observed in the most deformed area of tensile specimen (Figure 7a). These bands occurred with an angle of about 45° to the drawing direction and were probably due to the crosslinking points in pPLA that may locally limit chain drawability. From the present studies, the exact interaction between the shear bands and the cracking could not be clarified. Nevertheless, it is expected that the millimeter shear bands contain the sub-micrometer cracks.

3.4. Inclusion Structure Model

Based on STXM/NEXAFS, AFM, and µCT results, the structure of the plasticizer inclusions in pPLA was represented in **Figure 8** before and after drawing. At the nondeformed state, the inclusions had a shell structure rich in poly(acrylPEG) that was grafted/crosslinked to PLA matrix, while the core structure of the inclusions contained less poly(acrylPEG) compared to the shell (Figure 8a). After drawing, the poly(acrylPEG) domains of the inclusions were stretched so that the local density became lower in the core as well as in the shell (Figure 8b). Last, cracks bridging inclusions also appeared with the imposed strain probably due to the presence of crosslinking points.

4. Conclusions

The objectives of this work were to identify the chemical structure of inclusions, which were formed during a reactive extrusion process, and to identify the deformation mechanisms of these inclusions. As a case study, polylactide (PLA) plasticized with acrylated poly(ethylene glycol) (acrylPEG) in the presence of a free radical initiator was chosen. The structure of plasticized PLA by reactive extrusion (pPLA) was resolved by combining STXM coupled with NEXAFS nanospectroscopy and AFM with elastic modulus mapping. µCT analyses were done as a complementary structural investigation.

It was found that the inclusions in pPLA had a core–shell morphology with poly(acrylPEG)-rich domains at the shell

and poly(acrylPEG)-poor domains at the core. Note that the polymerization of initial acrylPEG was proved by an increase of the inclusion elastic modulus from the plasticized PLA obtained by a simple mixing between PLA and acrylPEG (PLA/acrylPEG) to pPLA. NEXAFS results also indicate a polymerization of acrylPEG since the absorption spectrum of pPLA inclusions was similar to the absorption spectrum of polymerized acrylPEG (poly(acrylPEG)). The core–shell morphology of the inclusions has been explained by two mechanisms: (i) the formation of plasticizer agglomerates and (ii) a higher chemical reactivity at the agglomerate–matrix interface compared to the inclusion core due to the presence of free radicals engendered from the radical initiator, acrylPEG, and PLA. After drawing, the inclusions were elongated so that the local density dropped but without exhibiting internal voiding. Furthermore, no inclusion–matrix debonding was noted. These findings demonstrated that the deformation mechanisms of the pPLA inclusions may enhance the plasticity of the material since no damage occurred. On the other hand, sub-micrometer cracks bridging neighboring inclusions were observed. Despite the detrimental aspect of cracking, cracks in pPLA were localized between inclusions and did not further propagate, which is believed to be suitable to ensure a good plasticity.

The developed reactive plasticization of PLA avoids plasticizer leaching and provides a material with improved toughness compared to the reference PLA matrix. However, it appears that cracks were generated at the inclusion–matrix interface upon drawing. It is hypothesized that crosslinking points present at this interface restrict chain mobility and hence engender crack development. A comprehensive study of the chemical reactions occurring at the inclusion–matrix interface should be done to better control the crosslinking density of this region and, hence, to further optimize the dissipation of stress.

Conflict of Interest

The authors declare no conflict of interest.

[1] G. H. Hu, S. Hoppe, L. L. Feng, C. Fonteix, in *Mixing and Compounding of Polymers*, 2nd ed. (Ed: I. Manas-Zloczower), Carl Hanser Verlag, München **2009**, pp. 1019–1080.

[2] T. Sakai, in *Mixing and Compounding of Polymers*, 2nd ed. (Ed: I. Manas-Zloczower), Carl Hanser Verlag, München **2009**, pp. 981–1017.

[3] P. Cassagnau, V. Bounor-Legaré, F. Fenouillot, *Int. Polym. Process.* **2007**, *22*, 218.

[4] F. Hassouna, J.-M. Raquez, F. Addiego, V. Toniazzo, P. Dubois, D. Ruch, *Eur. Polym. J.* **2012**, *48*, 404.

[5] G. Kfoury, F. Hassouna, J.-M. Raquez, V. Toniazzo, D. Ruch, P. Dubois, *Macromol. Mater. Eng.* **2014**, *299*, 583.

[6] K. Choi, M.-C. Choi, D.-H. Han, T.-S. Park, C.-S. Ha, *Eur. Polym. J.* **2013**, *49*, 2356.

[7] B. Brüster, F. Addiego, F. Hassouna, D. Ruch, J.-M. Raquez, P. Dubois, *Polym. Degrad. Stab.* **2016**, *131*, 132.

[8] A. M. Donald, E. J. Kramer, *J. Mater. Sci.* **1982**, *17*, 2351.

[9] S. Cai, C. Zeng, N. Zhang, J. Li, M. Meyer, R. H. Fink, D. Shi, J. Ren, *RSC Adv.* **2016**, *6*, 25531.

[10] D. G. Yablon, A. Gannepalli, R. Proksch, J. Killgore, D. C. Hurley, J. Grabowski, A. H. Tsou, *Macromolecules.* **2012**, *45*, 4363.

[11] B. E. W. Fischer, H. J. Sterzel, G. Wegner, *Kolloid Z. Z. Polym.* **1973**, *251*, 980.

[12] J. Raabe, G. Tzvetkov, U. Flechsig, M. Böge, A. Jaggi, B. Sarafimov, M. G. C. Vernooij, T. Huthwelker, H. Ade, D. Kilcoyne, T. Tyliszczak, R. H. Fink, C. Quitmann, *Rev. Sci. Instrum.* **2008**, *79*, 113704.

[13] B. Watts, C. R. McNeill, J. Raabe, *Synth. Met.* **2012**, *161*, 2516.

[14] G. Kfoury, J.-M. Raquez, F. Hassouna, P. Leclère, V. Toniazzo, D. Ruch, P. Dubois, *Polym. Eng. Sci.* **2015**, *55*, 1408.

[15] B. O. Leung, A. P. Hitchcock, R. Cornelius, J. L. Brash, A. Scholl, A. Doran, *Biomacromolecules* **2009**, *10*, 1838.

[16] A. Schöll, R. Fink, E. Umbach, G. E. Mitchell, S. G. Urquhart, H. Ade, *Chem. Phys. Lett.* **2003**, *370*, 834.

[17] O. Dhez, H. Ade, S. G. Urquhart, *J. Electron Spectrosc. Relat. Phenom.* **2003**, *128*, 85.

[18] M. Zwahlen, S. Herrwerth, W. Eck, M. Grunze, G. Hähner, *Langmuir* **2003**, *19*, 9305.

[19] D. J. Menzies, B. Cowie, C. Fong, J. S. Forsythe, T. R. Gengenbach, K. M. McLean, L. Puskar, M. Textor, L. Thomsen, M. Tobin, B. W. Muir, *Langmuir* **2010**, *26*, 13987.

[20] J. Stöhr, *NEXAFS Spectroscopy*, Springer, Heidelberg **1992**.

[21] K. Wang, B. Brüster, F. Addiego, G. Kfoury, F. Hassouna, D. Ruch, J.-M. Raquez, P. Dubois, *Polym. Int.* **2015**, *64*, 1544.

[22] G. J. Salomons, M. A. Singh, T. Bardouille, W. A. Foran, M. S. Capel, *J. Appl. Crystallogr.* **1999**, *32*, 71.

[23] G. Stoclet, J. M. Lefebvre, R. Séguéla, C. Vanmansart, *Polymer* **2014**, *55*, 1817.

[24] M. Kowalczyk, E. Piorkowska, *J. Appl. Polym. Sci.* **2011**, *124*, 4579.

[25] L. L. Berger, E. J. Kramer, *J. Mater. Sci.* **1988**, *23*, 3536.